4

# Identification of Vulnerable Plaques with Optical Coherence Tomography

Takashi Kubo and Takashi Akasaka
*Wakayama Medical University*
*Japan*

## 1. Introduction

Recent advances in intravascular imaging have significantly improved the ability to detect high-risk, or vulnerable, plaque in vivo. Optical coherence tomography (OCT) is a new intravascular imaging method using a fiber-optic technology. The greatest advantage of OCT is its extraordinary high-resolution about 10-20 μm, which is approximately 10 times higher than that of intravascular ultrasound (IVUS). The high resolution afforded by this imaging modality is giving new insights into atherosclerotic plaque and the vascular responses after percutaneous coronary intervention (PCI). This report reviews the possibility of OCT for identification of vulnerable plaques in vivo.

## 2. Vulnerable plaque and pathology

The term "vulnerable plaque" is used to describe thrombosis prone plaques. Plaque rupture is the most frequent cause of coronary thrombosis, accounting for 60-65% for all coronary thrombi. The precursor lesion for plaque rupture is characterized by a thin fibrous cap heavily infiltrated macrophages and an underlying necrotic core. Virmani et al defined plaque vulnerability based on the actual thickness of the histological section from measurements made of plaque ruptures. The thin-cap fibroatheroma (TCFA) was defined as a lesion with a fibrous cap < 65 μm thick. A thickness of 65 μm was chosen as a criterion of instability because in rupture the mean cap thickness was 23 ± 19 μm; 95% of caps measured less than 65 μm within a limit of only two standard deviations. In addition to plaque rupture, plaque erosion can also result in coronary thrombosis. Erosion is usually found in the lesion with intimal thickening or thick-cap fibroatheroma. The thick fibrous cap in contrast to thin fibrous cap contains abundance of smooth muscle cells, proteoglycans and type III collagen but very few inflammatory cells.

## 3. Current OCT technology

OCT is an optical analogue of IVUS using near-infrared light. The wavelength used is 1,310 nm, which minimizes absorption of the light waves by water, protein, lipids, and hemoglobin without tissue damage. Based on the principles of low-coherence interferometry, the OCT system produces images with an axial resolution of 10-20 μm and a

lateral resolution of 25-30 μm (Table 1). An optic probe, with dimensions similar to those of a coronary guide wire, delivers light to the tissue and collects the light reflected from the tissue. The image wire of current time-domain OCT system (M2/M3 TD-OCT imaging system, LightLab Imaging, Inc., Westford, Massachusetts) consists of a 0.006 inch (0.15 mm) fiber-optic core that rotates inside a sheath with a diameter of 0.016 inch (0.41 mm) (Figure 1). Because the near-infrared light signals are attenuated by red blood cells, OCT needs a blood-free imaging zone. To remove blood from the coronary artery and deliver the image wire, an over-the-wire occlusion balloon catheter is used. The diameter of the catheter shaft is 4.4 Fr and the balloon, designed for low-pressure inflation, was thin-walled polyurethane with a diameter of 3.8 mm at 0.3 atmospheres (< 8.5 mm at 1.0 atmospheres) and a length of 6.5 mm. Lactated Ringer's flushing solution is injected through the central inner lumen, which is shared with the image wire, and exits from the distal tip. The OCT imaging procedure starts with advancing the tip of a 0.014 inch (0.36 mm) coronary guide wire into the distal coronary artery. The occlusion catheter is then advanced over the wire until the balloon is positioned proximal to the target lesion. After the guide wire and OCT image wire are exchanged, lactated Ringer's solution is continuously flushed through the central lumen of the occlusion catheter by a power injector, and the balloon is inflated gradually by a custom inflation device until blood flow is fully occluded. Motorized pullback OCT imaging is performed at a rate of 1.0 mm/sec for a length of 30 mm. Images are acquired at 15 frames/sec and are digitally archived. The images are saved in the OCT imaging system console. During the procedure, electrocardiographic and hemodynamic features should be carefully monitored. Yamaguchi et al evaluated the safety and feasibility of OCT in 76 patients with coronary artery disease. Procedural success rates were 97%, and significant adverse cardiac events, including vessel dissection, acute myocardial infarction or fatal arrhythmia, were not observed. An inherent limitation of OCT is need for a blood-free imaging zone. The coronary occlusion for OCT image acquisition limits evaluation of left main or ostial coronary lesions. In addition, the time constraint imposed by blood flow interruption as well as slow frame rate of current OCT system prevents scanning of a significant length of a coronary artery during a single flush.

Recently, a second-generation OCT technology, termed Fourier-domain OCT (C7 FD-OCT imaging system, LightLab Imaging, Inc., Westford, Massachusetts), has been developed that solves the current time-domain OCT problems by imaging at much higher frame rates (100 frame/sec), a faster pullback speed (20 mm/sec), and a wider scan diameter (8.3mm) without loss of image quality (Table 2). These advantages result from the elimination of mechanical scanning of the reference mirror and signal-to-noise advantages of Fourier-domain signal processing (Figure 2). Imaging catheter of Fourier-domain OCT (Dragonfly Imaging Catheter, LightLab Imaging, Inc., Westford, Massachusetts), which is designed for rapid-exchange delivery, has 2.5-2.8 Fr crossing profile and can be delivered over a 0.014-inch guidewire through a 6 Fr or larger guide catheter. Injecting angiographic contrast media, or a mixture of commercially available dextran 40 and lactated Ringer's solution (low-molecular-weight Dextran L Injection, Otsuka Pharmaceutical Factory, Tokushima, Japan) through the guide catheter (4-6 ml/sec, 2-3 second) can achieve effective clearing of blood for Fourier-domain OCT imaging. The high frame rate and fast pullback speed of Fourier-domain OCT allows to image long coronary segments with minimal ischemia, eliminating the need for proximal vessel balloon occlusion during image acquisition.

| | OCT | IVUS | Angioscopy | Angiography |
|---|---|---|---|---|
| Resolution (μm) | 10-20 | 80-120 | 10-50 | 100-200 |
| Probe size (mm) | 0.016 | 0.7 | 0.8 | n/a |
| Type of radiation | Near-IR light | Ultrasound | Visible light | X-ray |
| Other | Sub-surface tomogram | Sub-surface tomogram | Surface imaging only | Images of blood flow |

Table 1. Comparison of the characteristics of coronary imaging methods.

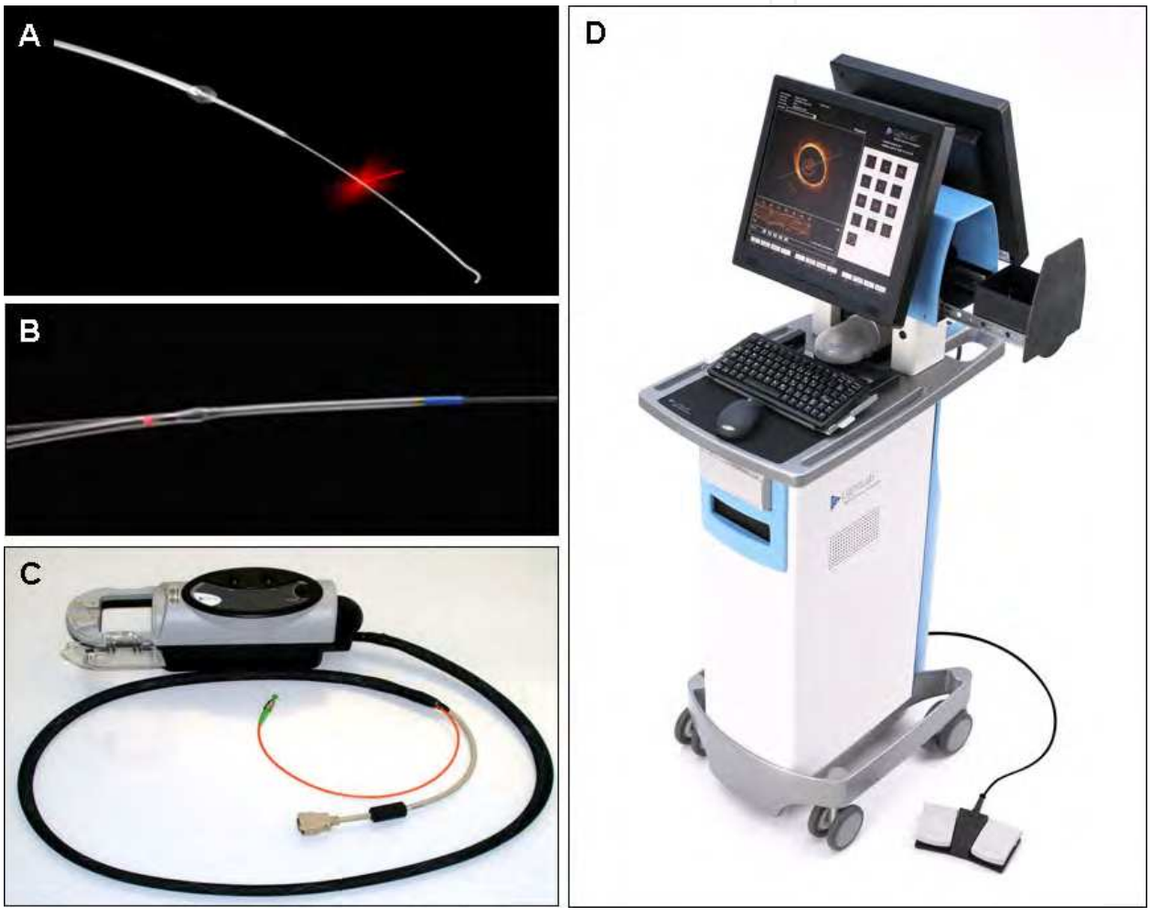


Fig. 1. LightLab OCT imaging system. (A) Time-domain OCT imaging wire. The time-domain OCT system employs a 0.016-inch fiber-optic imaging wire. (B) Fourier-domain OCT imaging catheter. Imaging catheter of Fourier-domain OCT has 2.5-2.8 Fr crossing profile and can be delivered over a 0.014-inch guidewire. (C) Patient interface unit. (D) OCT system console.

| | Time-domain OCT | Fourier-domain OCT |
|---|---|---|
| Axial resolution (μm) | 10-20 | 10-20 |
| Lateral resolution (μm) | 25-30 | 25-30 |
| Scan diameter (mm) | 6.8 | 8.3 |
| Frame rate (f/sec) | 15-20 | 100 |
| Number of lines (/frame) | 200-240 | 450 |
| Maximum pullback speed (mm/sec) | 2-3 | 20 |
| Coronary occlusion for imaging | Required | Not required |

Table 2. Performance of Fourier-domain OCT system in comparison with time-domain OCT System.

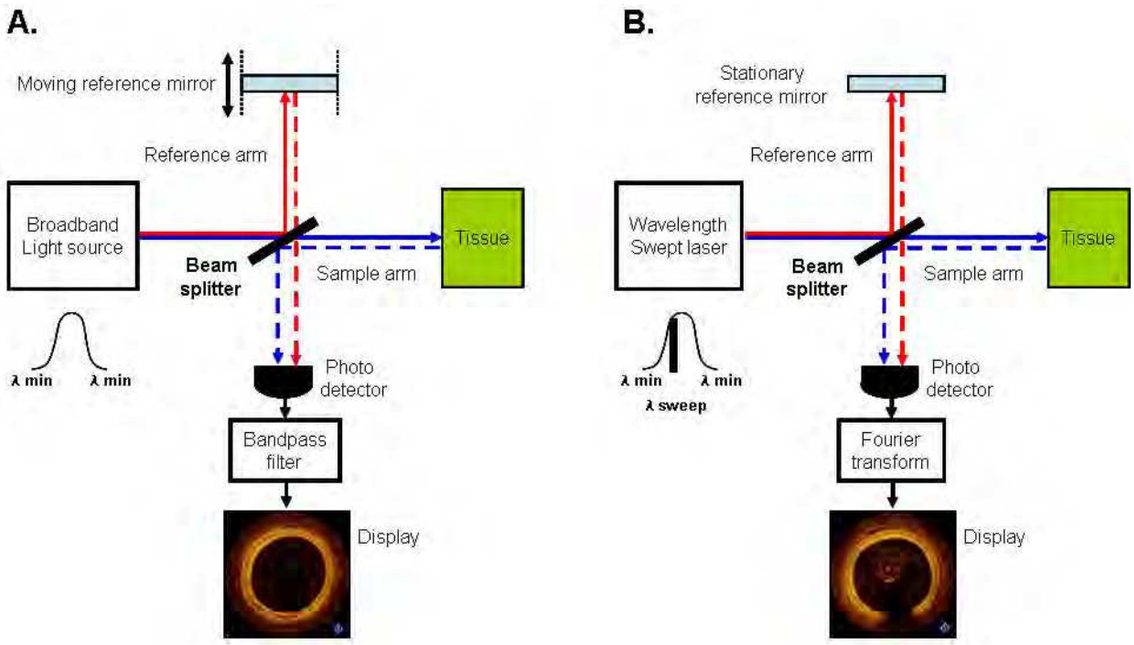


Fig. 2. Main components of time-domain OCT and Fourier-domain OCT. (A) In time-domain OCT, a broadband light source is divided by a beam splitter; part is sent to the tissue sample down the sample or measurement arm and the other down the reference arm to a moving mirror. The reflected signals are overlaid on a photo-detector. The intensity of interference is detected and used to create images. (B) In Fourier-domain OCT, the reference mirror does not move and the light source is a laser that sweeps its output rapidly over a broad band of wavelengths. Fourier transformation of the interference signals stored during a single sweep reconstructs the amplitude profile of the reflections, analogous to a single A-line in an ultrasound scan. Lasers with narrow line widths and wide sweep ranges enable the acquisition of Fourier-domain OCT images with high resolution over a wide range of depths.

## 4. Plaque characterization

Several histological examinations have demonstrated that OCT is highly sensitive and specific for plaque characterization. The high resolution of OCT allows us to identify 3-layer of coronary artery wall. In the OCT image, intima is observed as a signal rich layer nearest

the lumen, media is visualized as a signal poor middle layer, and adventitia is identified as a signal-rich outer layer of artery wall (Figure 3). OCT enables more accurate estimation of the intimal thickness in comparison with IVUS which can not distinguish the boundary of the intima and media. Kume et al compared the coronary intima – media thickness and the intimal thickness of 54 coronary arterial segments evaluated by histological examination with the results of OCT and IVUS. There was a better agreement in intima – media thickness between OCT and histological examination than between IVUS and histological examination ($r=0.95$, $p<0.001$, mean difference = –0.01 ± 0.07 mm for OCT; $r=0.88$, $p<0.001$, mean difference = –0.03 ± 0.10 mm for IVUS). Moreover, there was an excellent agreement in the intimal thickness between OCT and histological examination ($r=0.98$, $p<0.001$, mean difference = 0.01 ± 0.04 mm).

Yabushita el al developed objective OCT image criteria for differentiating distinct components of atherosclerotic tissue. In their histology-controlled OCT study with 357 autopsy segments from 90 cadavers, fibrous plaques were characterized by homogeneous signal-rich regions (Figure 4), fibrocalcific plaques by signal-poor regions with sharp borders (Figure 5), and lipid-rich plaques by signal-poor regions with diffuse borders (Figure 6). Validation test revealed good intra- and inter-observer reliability ($\kappa$ = 0.83–0.84) as well as excellent sensitivity and specificity—71–79% and 97–98% for fibrous plaques, 95–96% and 97% for fibrocalcific plaques, and 90–94% and 90–92% for lipid-rich plaques, respectively. These definitions have formed the basis of plaque composition interpretation (Table 3). Using these definitions, Kawasaki et al studied 128 coronary arterial sites from 42 coronary arteries of 17 cadavers by using OCT, integrated backscatter IVUS and conventional IVUS, and reported that OCT has a best potential for tissue characterization of coronary plaques (Fibrous tissue: sensitivity—98% vs. 94% vs. 93%, specificity—94% vs. 84% vs. 61%; Calcification: sensitivity—100% vs. 100% vs. 100%, specificity—100% vs. 99% vs. 99%; lipid pool: sensitivity—95% vs. 84% vs. 67%, specificity—98% vs. 97% vs. 95%). Kume et al also examined 166 sections from 108 coronary arterial segments of 40 consecutive human cadavers by using OCT and IVUS, and showed that OCT had a higher sensitivity for characterizing lipid-rich plaques than IVUS (85% vs. 59%, $p=0.030$). The intraobserver and interobserver agreement of OCT for characterizing plaque type was high ($\kappa=0.92$ and $\kappa=0.86$, respectively). These results suggest the possibility of OCT to identify vulnerable plaques which might contain lipid-rich necrotic core.

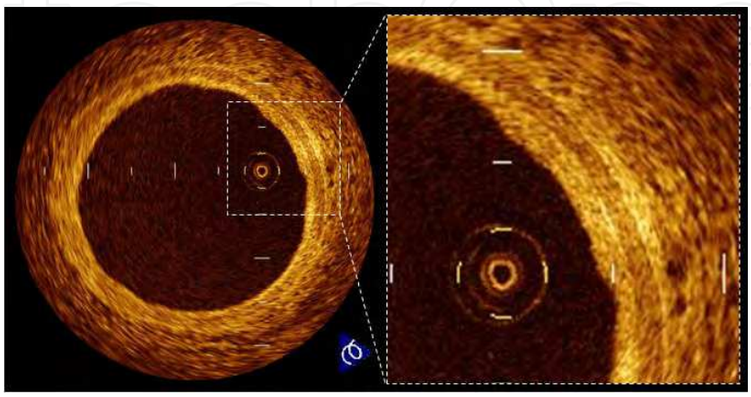

Fig. 3. Normal coronary wall. OCT image of normal coronary artery showing good contrast of the layers of the vessel wall including intima, media and adventitia.

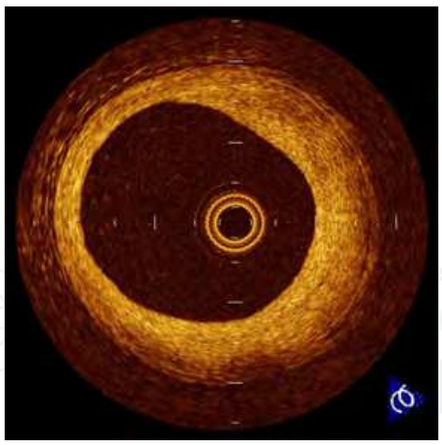

Fig. 4. Fibrous plaque. OCT image of a fibrous coronary plaque showing a homogeneous, signal-rich interior.

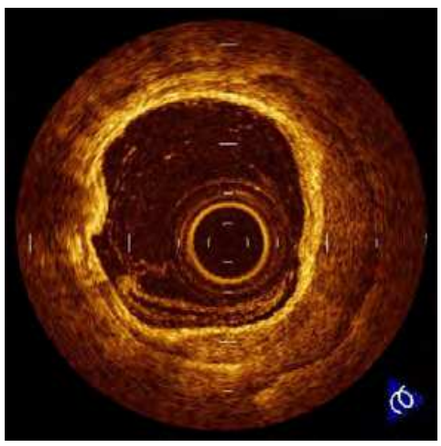

Fig. 5. Fibrocalcific plaque. OCT image of a fibrocalcific coronary plaque showing a sharply delineated region with a signal-poor interior.

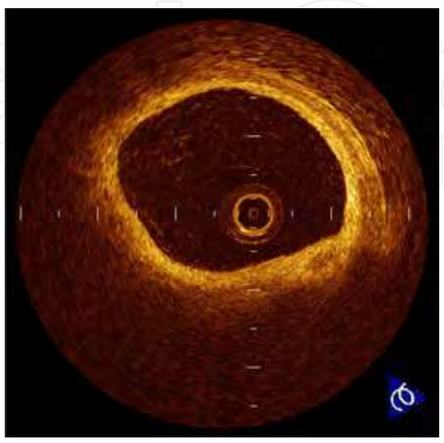

Fig. 6. Lipid-rich plaque. OCT image of a lipid-rich plaque showing a signal-poor lipid pool with poorly delineated borders beneath a homogeneous band, corresponding to fibrous cap.

| Histology | OCT findings |
|---|---|
| Intima | Signal-rich layer near lumen |
| Media | Signal-poor layer in middle of artery wall |
| Adventitia | Signal-rich outer layer of artery wall |
| Fibrous tissue | Signal-rich, homogenous area |
| Calcium | Well-demarcated, heterogeneous area |
| Lipid | Signal-poor, poorly demarcated, homogenous area |
| Fibrous-cap | Signal-rich layer overlying signal-poor area |

Table 3. OCT Characteristics of coronary microstructures

## 5. Vulnerable plaque detection

Since OCT has a near-histological grade resolution, many in-vitro and in vivo studies have been done to validate the capability of OCT to visualize vulnerable plaque features.

### 5.1 Plaque rupture and erosion

OCT can detect plaque rupture (Figure 7) and erosion (Figure 8) more precisely in comparison with conventional intravascular imaging techniques. Kubo et al used OCT, IVUS and angioscopy in patients with acute myocardial infarction (AMI) to assess the ability of each imaging method to detect the specific characteristics of vulnerable plaque. OCT was superior in detecting plaque rupture (73% vs. 40% vs. 43%, p=0.021), erosion (23% vs. 0% vs. 3%, p=0.003) and thrombus (100% vs. 33% vs. 100%, p<0.001) as compared with IVUS and angioscopy. Intra- and inter-observer variability of OCT yielded acceptable concordance for these characteristics (κ=0.61–0.83).

Using the capability of OCT for assessing plaque rupture and erosion in vivo, several studies have been performed to understand the mechanisms of acute coronary syndrome (ACS). Tanaka et al used OCT to investigate the relationship in patients with ACS between the morphology of a ruptured plaque and the patient's activity at the onset of ACS. Their data revealed that the thickness of the broken fibrous cap in the exertion group was significantly higher than in the rest-onset group (rest onset: 50 μm [interquartile median 15 μm]; exertion: 90 μm [interquartile median 65 μm], p<0.001), and some plaque rupture occurred in thick fibrous caps of > 65 μm depending on exertion levels. Mizukoshi et al used OCT to assess the relationship between clinical presentation and plaque morphologies in patients with unstable angina pectoris (UAP). In comparison with the Braunwald class I or II UAP patients, class III UAP patients had the highest frequency of plaque rupture (class I, 43%; class II, 13%; class III, 71%; p<0.001) and the thinnest fibrous cap (class I, median = 140 μm, quartile 1 to 3 = 90 to 160; class II, 150 μm, 120 to 160; class III, 60 μm, 40 to 105; p<0.001). In addition, class I UAP patients had the highest frequency of plaque erosion (class I, 32%; class II, 7%; class III, 8%; p=0.003) and the smallest minimum lumen area (class I, median 0.70 $mm^2$, quartiles 1 to 3 = 0.42 to 1.00; class II, 1.80 $mm^2$, 1.50 to 2.50; class III, 2.31 $mm^2$, 1.21 to 3.00; p<0.001). Recently, Ino et al used OCT to investigate the difference of culprit lesion morphologies between ST-segment elevation myocardial infraction (STEMI) and non–ST-segment elevation ACS (NSTEACS). The incidence of plaque rupture was significantly higher in STEMI compared with NSTEACS (70% vs. 47%, p=0.033). Although the lumen area at the site of plaque rupture was similar in the both groups, the area of ruptured cavity was significantly larger in STEMI compared with NSTEACS (2.52 ± 1.36

$mm^2$ vs. 1.67 ± 1.37 $mm^2$, p=0.034). Furthermore, the ruptured plaque of which aperture was open-wide against the direction of coronary flow was more often seen in STEMI compared with NSTEACS (46% vs. 17%, p=0.036).

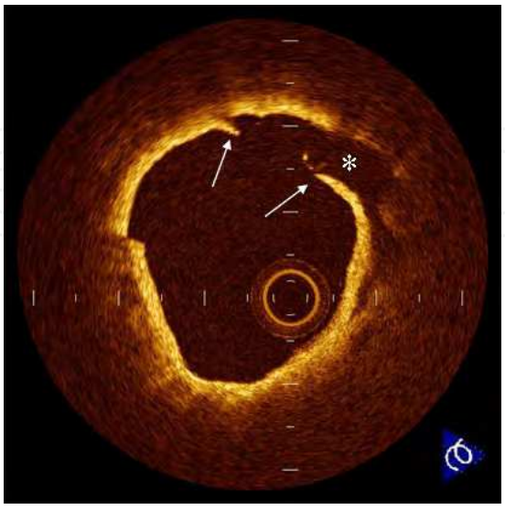

Fig. 7. Plaque rupture. Plaque rupture is defined as the presence of fibrous-cap discontinuity (arrows) and a cavity formation (*) in the plaque.

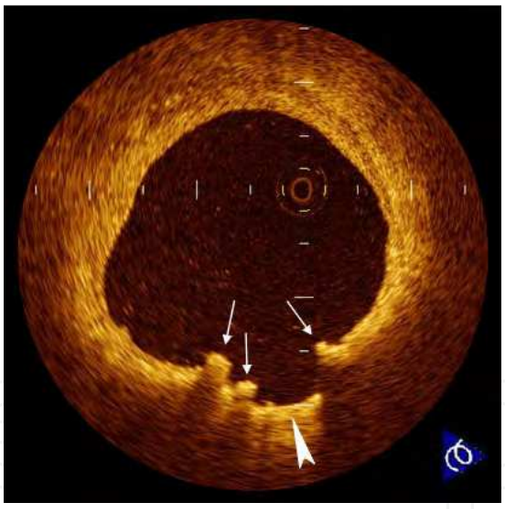

Fig. 8. Plaque erosion. Erosion (arrowhead) is usually comprised of OCT evidence of thrombi (arrows), an irregular luminal surface, and no evidence of cap rupture evaluated in multiple adjacent frames.

### 5.2 Thin-cap fibroatheroma

OCT might be the best tool available to detect TCFAs in vivo (Figure 9). Kume et al examined the reliability of OCT for measuring the fibrous cap thickness. In the examination of 35 lipid-rich plaques from 38 human cadavers, there was a good correlation of the fibrous cap thickness between OCT and histological examination ($r = 0.90$; $p<0.001$). In the clinical setting, Sawada et al compared the feasibility for detecting TCFA between OCT and virtual

histology IVUS. Although the positive ratio of virtual histology IVUS for detecting TCFA was 45.9%, that of OCT was 77.8%. Jang et al analyzed OCT images among 57 patients who presented with stable angina pectoris (SAP), ACS, or AMI. The AMI group was more likely than the ACS group, who was more likely than the SAP group, to have a thinner cap, more lipid, and a higher percentage of TCFA (72% vs. 50% vs. 20%, respectively, p = 0.012). On top of its reliability as a tool to measure the fibrous-cap thickness in vivo, a recent OCT study conducted by Takarada et al demonstrated that the lipid-lowering therapy with statin for 9 months follow-up significantly increased the fibrous-cap thickness in patients with hypercholesterolemia (151 ± 110 to 280 ± 120 μm, p<0.01). As therapies to prevent or make regression of atherosclerosis are developed, OCT can help to assess the treatment efficacy.

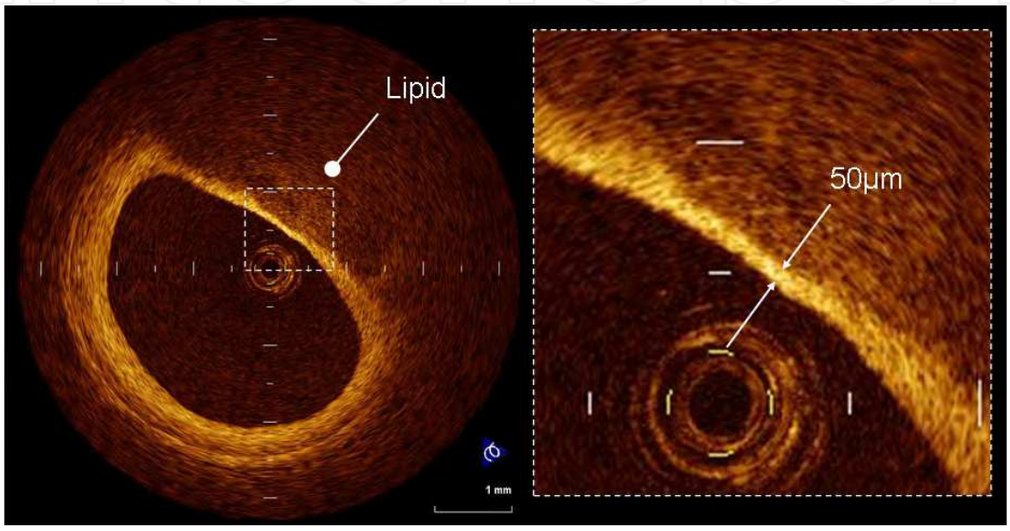


Fig. 9. Thin-cap fibroatheroma. A fibrous cap is identified as a signal-rich homogenous region overlying a lipid core, which is characterized by a signal-poor region in the OCT image. Thin-cap fibroatheroma is defined as a plaque with a fibrous cap measuring <65 μm.

### 5.3 Thrombus

The OCT characteristics of coronary thrombi were studied by Kume et al in 108 coronary arterial segments at postmortem examination. Red thrombus (Figure 10-A), which mainly consists of red-blood cell, is identified as high-backscattering protrusions inside the lumen of the artery with signal-free shadow, while white thrombus (Figure 10-B), which mainly consists of platelet and fibrin, is identified as signal-rich, low-backscattering protrusions in the OCT image. Using a measurement of the OCT signal attenuation within the thrombus, the authors demonstrated that a cut-off value of 250 μm in the 1/2 width of signal attenuation can differentiate white from red thrombi with a high sensitivity (90%) and specificity (88%).

### 5.4 Plaque neovascularization

Plaque neovascularization is a common feature of vulnerable plaque. Proliferation of micro-vessels is considered to be related with intraplaque haemorrhage and plaque destabilization. The high resolution of OCT provides an opportunity to detect plaque neovascularization in vivo (Figure 11). Kitabata et al demonstrated increase of micro-vessels density in TCFAs by

using OCT. The presence of micro-vessels in the plaques was also associated with positive vessel remodeling and elevated hs-CRP levels. The OCT evaluation of micro-vessels density might be helpful to assess plaque vulnerability.

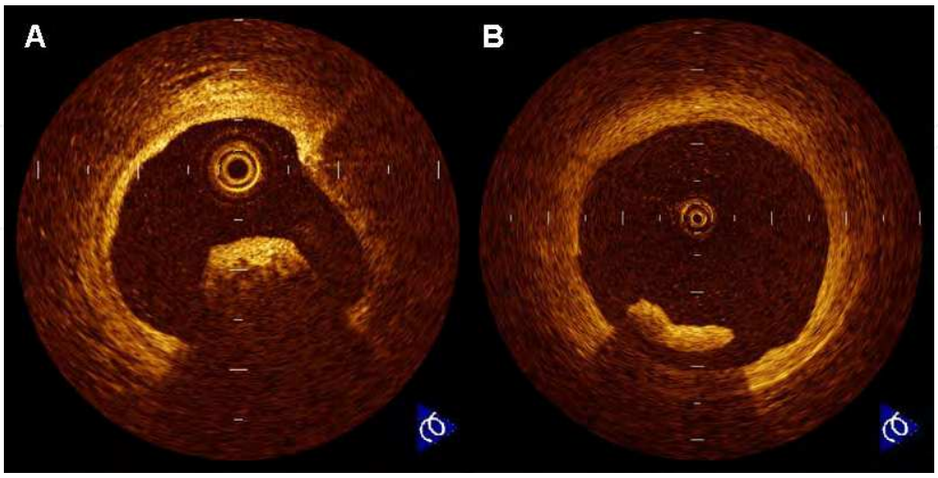


Fig. 10. Intracoronary thrombi. (A) Red thrombus is defined as a protrusion inside the lumen of the artery with high signal attenuation in the OCT image. (B) White thrombus is defined as a protruding mass with low signal attenuation in the OCT image.

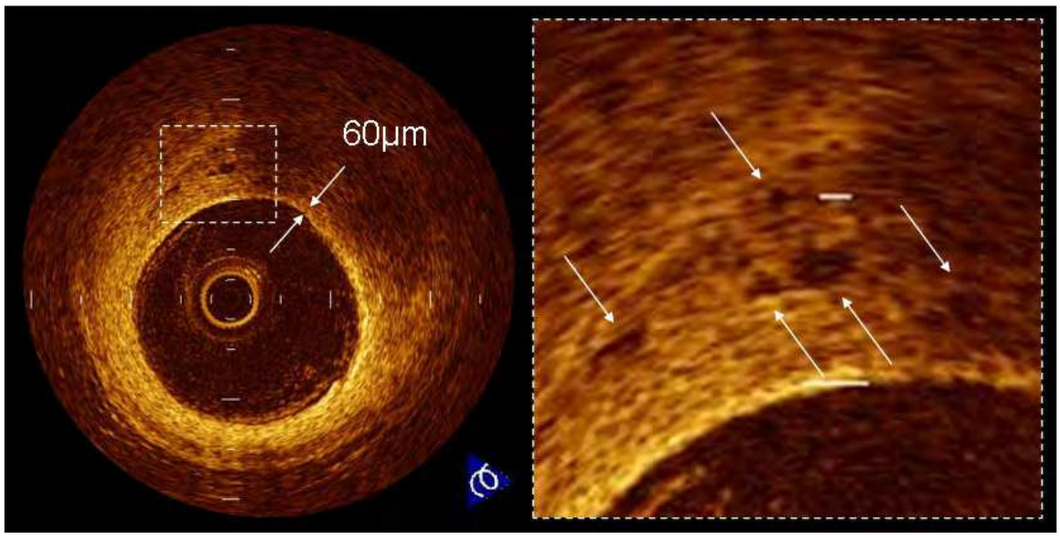


Fig. 11. Micro-vessels in the coronary plaque. Vessels within the intima (arrows) appear as signal poor voids that are sharply delineated.

### 5.5 Macrophages

A unique aspect of OCT is its ability to visualize the macrophages (Figure 12). Tearney et al proposed the potential of OCT to assess macrophage distribution within fibrous caps. There was a high degree of positive correlation between OCT and histological measurements of fibrous cap macrophage density ($r<0.84$, $P<0.001$). A range of OCT signal standard deviation

thresholds (6.15% to 6.35%) yielded 100% sensitivity and specificity for identifying caps containing >10% CD68 staining.

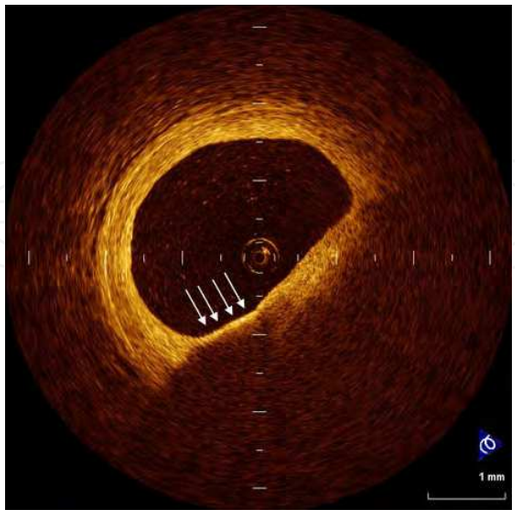


Fig. 12. Macrophage. Macrophages (arrows) are seen as signal-rich, distinct or confluent punctuate regions that exceed the intensity of background speckle noise.

## 6. Multiple lesion instability

In the diffuse nature of coronary atherosclerosis, plaque instability might be expected to develop in a multifocal pattern. Virmani et al showed that 70% of cases of sudden cardiac death had non-ruptured TCFAs. Most non-ruptured TCFAs and ruptured plaque are localized in the proximal 1/3 of the major coronary arteries. In a 3-vessel VH–IVUS study, Hong et al demonstrated that 72% of patients with AMI or UAP had multiple VH–IVUS-derived TCFAs. Asakura et al performed 3-vessel angioscopic examination in AMI and showed that yellow plaques were equally prevalent in the infarct-related and non-infarct-related coronary arteries. In the multifocal OCT study, Tanaka et al reported that 7% of patients with acute coronary syndrome had >2 OCT-derived TCFAs in the entire culprit coronary artery. Kubo et al evaluated non-culprit vessels by using OCT and demonstrated a greater frequency of multiple OCT-derived TCFAs in AMI patients than in SAP patients. Fujii et al performed a prospective OCT analysis of all 3 major coronary arteries to evaluate the incidence and predictors of TCFAs in patients with AMI and SAP. Multiple TCFAs were observed more frequently in AMI patients than in SAP patients (69% vs. 10%, $p<0.001$). In the entire cohort, multivariate analysis revealed that the only independent predictor of TCFA was AMI (OR=4.12, 95% CI=2.35-9.87, p=0.020,). These OCT results support the theory that acute coronary syndrome is a multifocal process (Figure 13).

## 7. Drug-eluting stent in vulnerable lesion

Drug-eluting stent has been reported to impair local vascular healing with delayed endothelization. The patients with ACS present a higher risk for thrombotic complication after stent implantation in comparison with SAP. Therefore, vascular response after drug-eluting stent implantation in the vulnerable lesion is a great concern. Recently, Kubo et al used OCT to evaluate lesion morphologies after drug-eluting stent implantation in the

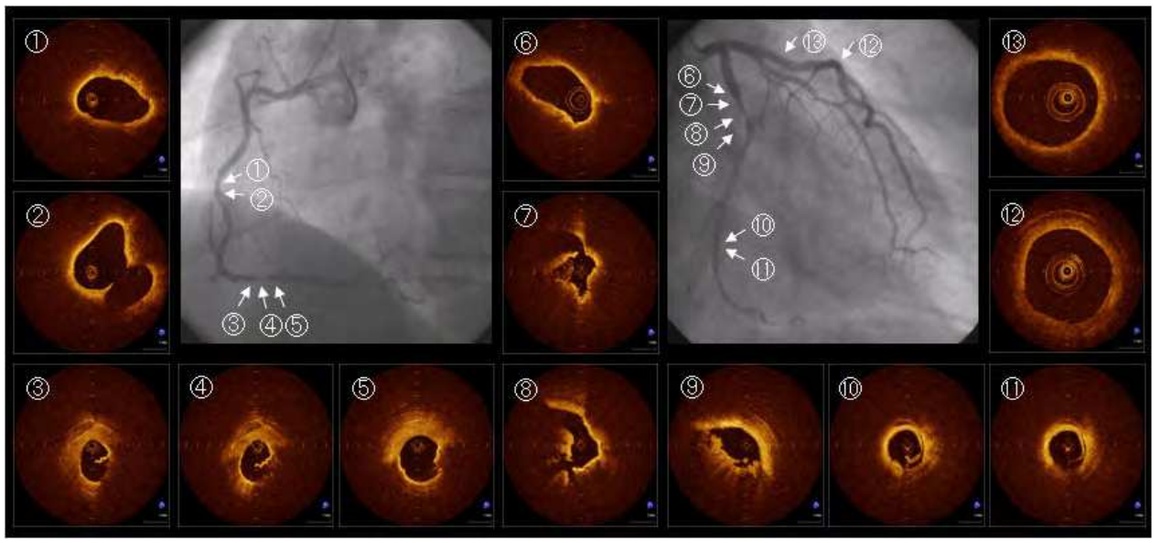


Fig. 13. Multiple lesion instability in patient with acute myocardial infarction. Coronary angiogram showed that the culprit lesion was located in the proximal site of left circumflex coronary artery (diameter stentosis = 99%; TIMI-II flow). Thin-cap fibroatheroma (⑥), plaque rupture (⑦, ⑧) and intracoronary thrombi (⑦, ⑧) were observed at the culprit lesion by OCT. Although the plaques in left descending coronary artery (⑫, ⑬) were not unstable, thin-cap fibroatheroma (①-⑤) and plaque rupture (③, ④, ⑤, ⑩, ⑪) was detected by OCT in the non-culprit lesions of right coronary artery and distal left circumflex coronary artery.

unstable lesions. Inadequate stent apposition (67% vs. 32%, p=0.038) and tissue protrusion (79% vs. 42%, p=0.005) after PCI were observed more frequently in UAP patients compared with SAP patients. Plaque rupture was significantly increased after PCI in UAP patients (42% to 75%, p=0.018). The persistence of core cavity after plaque rupture at 9 months' follow-up (Figure 14) was observed more frequently in UAP patients compared with SAP patients (28% vs. 4%, p=0.031). At 9 months' follow-up, the incidence of inadequately apposed stent (33% vs. 4%, p=0.012) and partially uncovered stent by neointima (72% vs. 37%, p=0.019) was significantly greater in UAP patients than that in SAP patients. Residual plaque rupture behind the stent and uncovered stent struts might be important risks for late stent thrombosis because the lipid content of exposed necrotic core and metal stent is highly thrombogenic (Figure 14). Although arterial healing with excessive neointimal growth leads to restenosis, neointima (or endothelium) that seals the underlying thrombogenic components may protect against late stent thrombosis.

## 8. Atherosclerotic changes in neointimal tissue inside stent

Atherosclerotic changes and consequent plaque vulnerability occur in the neointimal tissue inside the stent. Takano et al observed the neointimal characteristics of bare-metal stents in early phase (<6 months) and late phase (> 5 years) by using OCT. Lipid-rich neointima was often seen in the late phase compared with the early phase (67% vs. 0%, p<0.001). The appearance of intraintima neovascularization was more prevalent in the late phase than the early phase (62% vs. 0%, p<0.001). Kashiwagi et al used OCT to examine the stented

segments in cases with very late stent thrombosis, and reported neointimal plaque rupture. Atherosclerotic progression in neointimal tissue inside the stents might contribute to late clinical events after stent treatment (Figure 15).


Fig. 14. Residual plaque rupture behind coronary stent. The OCT image at 9-month follow-up after drug-eluting stent implantation shows persistence of core cavity and inadequately-apposed stent struts without neointimal coverage.

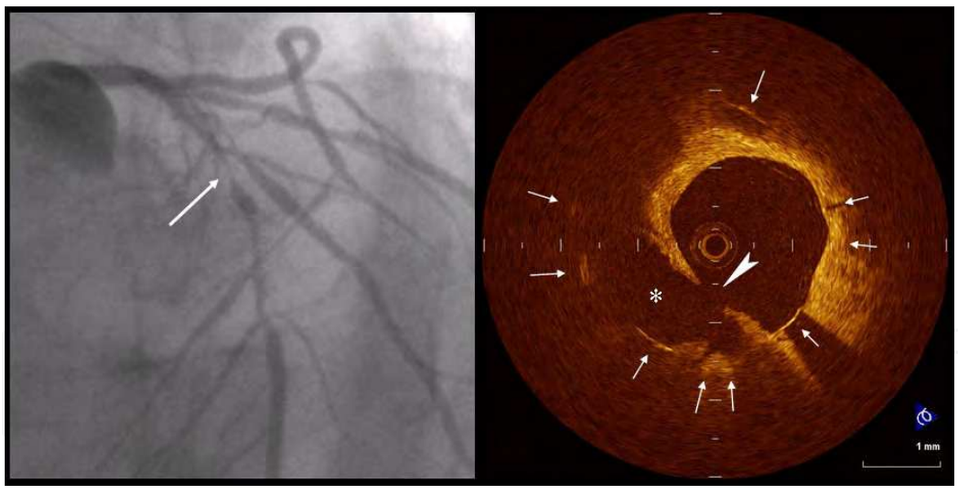


Fig. 15. A case with neointimal plaque rupture inside bare-metal stent. A 60-year-old man was given a diagnosis of stable angina and treated with a bare-metal stent (3.5 x 18 mm) deployed to the mid-portion of the left anterior descending artery 8 years ago. A follow-up coronary angiography at 6 months after the procedure presented no restenosis. Eight years after stent deployment, he suddenly suffered recurrence of angina and was admitted to the hospital. A coronary angiography showed severe in-stent restenosis of the previously stented segment of the LAD (arrow). Before any interventions, OCT was performed. OCT clearly revealed plaque rupture (arrowhead) and cavity formation (*) within well expanded stent struts (arrows).

## 9. Limitations

OCT has a relatively shallow axial penetration depth of 2mm. The OCT signal does not reach the back wall of thick atherosclerotic lesions. The penetration depth of OCT depends on tissue characteristics. Lipid-rich plaque or coronary thrombus causes OCT signal attenuation, which interrupts to observe deep layers of coronary artery wall. OCT is not appropriate for the visualization of whole vessel and the evaluation of arterial remodeling.

## 10. Current technology challenges

Recently, Tearney et al reported that Fourier-domain OCT, called optical frequency-domain imaging by author's group, enables imaging of the 3-dimensional microstructure of long segments of coronary arteries. In addition, Fourier-domain OCT facilitates the acquisition of spectroscopic and polarization, Doppler and other imaging modes for plaque characterization. When Fourier-domain OCT is fully exploited, it has the potential to dramatically change the way that physicians and researchers understand the coronary artery disease in order to better diagnose and treat disease.

## 11. Conclusion

The high resolution of OCT provides histology-grade definition of the microstructure of coronary plaque in vivo. OCT allows a greater understanding of the pathophysiology of vulnerable plaque. Whether OCT will have an established clinical role in vulnerable plaque detection must depend on the outcomes of future prospective natural history studies. Precise identification of thrombosis-prone vulnerable plaque could change our approach to the treatment of coronary atherosclerotic disease and contribute to prevention of ACS.

## 12. Acknowledgment

The authors thank Teruyoshi Kume, MD; Hironori Kitabata, MD; Yasushi Ino, MD; Takashi Tanimoto, MD; Kohei Ishibashi, MD; Yoshiki Matsuo, MD; Yasushi Okumoto, MD for assistance with OCT image acquisition and analysis.

## 13. References

Akasaka, T.; Kubo, T. & Mizukoshi, M. (2010). Pathophysiology of acute coronary syndrome assessed by optical coherence tomography. *J Cardiol*, Vol. 56, No.1, (July), pp. 8-14

Ino, Y.; Kubo, T. & Tanaka, A. (2011). Difference of culprit lesion morphologies between ST-segment elevation myocardial infarction and non-ST-segment elevation acute coronary syndrome: an optical coherence tomography study. *JACC Cardiovasc Interv,* Vol. 4, No.1, (January), pp. 76-82

Fujii, K.; Masutani. M. & Okumura, T. (2008). Frequency and predictor of coronary thin-cap fibroatheroma in patients with acute myocardial infarction and stable angina pectoris a 3-vessel optical coherence tomography study. *J Am Coll Cardiol,* Vol. 52, No.9, (August 26), pp. 787-788

Gonzalo, N.; Serruys, PW. & Okamura, T. (2009). Optical coherence tomography patterns of stent restenosis. *Am Heart J*, Vol. 158, No. 2, (August), pp. 284-293

Guagliumi, G.; Costa, MA. & Sirbu, V. (2011). Strut coverage and late malapposition with paclitaxel-eluting stents compared with bare metal stents in acute myocardial infarction: optical coherence tomography substudy of the Harmonizing Outcomes with Revascularization and Stents in Acute Myocardial Infarction (HORIZONS-AMI) Trial. *Circulation*, Vol. 123, No. 3, (January 25), pp. 274-281

Habara, M.; Terashima, M. & Nasu, K. (2011). Difference of tissue characteristics between early and very late restenosis lesions after bare-metal stent implantation: an optical coherence tomography study. *Circ Cardiovasc Interv*, Vo. 4, No. 3, (June), pp. 232-238

Jang, IK.; Tearney, GJ. & MacNeill, B. (2005). In vivo characterization of coronary atherosclerotic plaque by use of optical coherence tomography. *Circulation,* Vol. 111, No.12, (March 29), pp. 1551-1555

Kashiwagi, M.; Tanaka, A. & Kitabata, H. (2009). Relationship between coronary arterial remodeling, fibrous cap thickness and high-sensitivity C-reactive protein levels in patients with acute coronary syndrome. *Circ J,* Vol. 73, No.7, (July), pp. 1291-1295

Kashiwagi, M.; Tanaka, A. & Kitabata, H. (2009). Feasibility of noninvasive assessment of thin-cap fibroatheroma by multidetector computed tomography. *JACC Cardiovasc Imaging,* Vol. 2, No.12, (December), pp. 1412-1419

Kashiwagi, M.; Kitabata, H. & Tanaka, A. (2010). Very late clinical cardiac event after BMS implantation: in vivo optical coherence tomography examination. *JACC Cardiovasc Imaging,* Vol. 3, No.5, (May), pp. 525-527.

Kawasaki, M.; Bouma, BE. & Bressner, J. (2006). Diagnostic Accuracy of Optical Coherence Tom ography and Integrated Backscatter Intravascular Ultrasound Images for Tissue Characterization of Human Coronary Plaques. *J Am Coll Cardiol,* Vol. 48, No.1, (July 4), pp. 81-88

Kataiwa, H.; Tanaka, A. & Kitabata, H. (2008). Safety and usefulness of non-occlusion image acquisition technique for optical coherence tomography. *Circ J,* Vol. 72, No.9, (September), pp. 1536-1537

Kitabata, H.; Kubo, T. & Akasaka, T. (2008) Identification of multiple plaque ruptures by optical coherence tomography in a patient with acute myocardial infarction: a three-vessel study. *Heart.* Vol. 94, No.5, (May), pp. 544

Kitabata, H.; Tanaka, A. & Kubo, T. (2010). Relation of microchannel structure identified by optical coherence tomography to plaque vulnerability in patients with coronary artery disease. *Am J Cardiol,* Vol. 105, No.12, (Jun 15), pp. 1673-1678

Kubo, T.; Imanishi, T. & Takarada, S. (2007). Assessment of culprit lesion morphology in acute myocardial infarction: ability of optical coherence tomography compared with intravascular ultrasound and coronary angioscopy. *J Am Coll Cardiol,* Vol. 50, No.10, (September 4), pp. 933-939

Kubo, T.; Imanishi, T. & Takarada, S. (2008). Implication of plaque color classification for assessing plaque vulnerability: A coronary angioscopy and optical coherence tomography investigation. *JACC Cardiovasc Interv.* Vol. 1, No.1, (February), pp. 74-80.

Kubo, T.; Imanishi, T. & Takarada, S. (2008). Comparison of vascular response after sirolimus-eluting stent implantation between unstable angina pectoris and stable angina pectoris: a serial optical coherence tomography study. *JACC Cardiovasc Imaging,* Vol. 1, No.4, (July), pp. 475-484

Kubo, T. & Akasaka, T. (2009). Reply Letter to: Optical coherence tomography to diagnose under-expansion of a drug eluting stent. *JACC Cardiovasc Imaging,* Vol. 2, No.2, (February), pp. 246

Kubo, T. & Akasaka, T. (2008). Recent advances in intracoronary imaging techniques: focus on optical coherence tomography. *Expert Review of Medical Devices,* Vol.5, No.6, (November), pp. 691-697

Kubo, T.; Imanishi, T. & Kashiwagi, M. (2010). Multiple coronary lesion instability in patients with acute myocardial infarction as determined by optical coherence tomography. *Am J Cardiol,* Vol.105, No.3, (February), pp. 318-322

Kubo, T.; Xu, C. & Wang, Z. (2011). Plaque and Thrombus evaluation by Optical Coherence Tomography. *Int J Cardiovasc Imaging*, Vol. 27, No. 2, (February), pp. 289-298

Kubo, T.; Nakamura, N. & Matsuo, Y. (2011). Virtual histology intravascular ultrasound compared with optical coherence tomography for identification of thin-cap fibroatheroma. *Int Heart J*, Vol. 52, No. 3, (May), pp. 175-179

Kume, T; Akasaka, T. & Kawamoto, T. (2005). Assessment of coronary intima-media thickness by optical coherence tomography: comparison with intravascular ultrasound. *Circ J,* Vol. 69, No.8, (August), pp. 903-907

Kume, T; Akasaka, T. & Kawamoto, T. (2006). Assessment of Coronary Arterial Plaque by Optical Coherence Tomography. *Am J Cardiol,* Vol. 97, No.8, (April), pp. 1172-1175

Kume, T.; Akasaka, T. & Kawamoto, T. (2006). Assessment of coronary arterial thrombus by optical coherence tomography. *Am J Cardiol,* Vol. 97, No.2, (June), pp. 1713-1717

Kume, T.; Akasaka, T. & Kawamoto, T. (2006). Measurement of the thickness of the fibrous cap by optical coherence tomography. *Am Heart J,* Vol. 152, No.4, (October),pp. e1-4

Kume, T.; Okura, H. & Yamada, R. (2009). Frequency and spatial distribution of thin-cap fibroatheroma assessed by 3-vessel intravascular ultrasound and optical coherence tomography. *Circ J,* Vol. 73, No.6, (June), pp. 1086-1091

Liu, Y.; Imanishi, T. & Kubo, T. (2010). Assessment by optical coherence tomography of stent struts across side branch. -Comparison of bare-metal stents and drug-elution stents. *Circ J,* Vol. 75, No.1, (December 24), pp. 106-112

MacNeill, BD.; Jang, IK. & Bouma, BE. (2004). Focal and multi-focal plaque macrophage distributions in patients with acute and stable presentations of coronary artery disease. *J Am Coll Cardiol*, Vol. 44, No. 5, (September 1), pp. 972-979

Mizukoshi, M. Imanishi, T. & Tanaka, A. (2010). Clinical classification and plaque morphology determined by optical coherence tomography in unstable angina pectoris. *Am J Cardiol,* Vol. 106, No.3, (August), pp. 323-328

Nadkarni, SK.; Pierce, MC. & Park, BH. (2007). Measurement of collagen and smooth muscle cell content in atherosclerotic plaques using polarization-sensitive optical coherence tomography. *J Am Coll Cardiol,* Vol. 49, No.13, (April), pp. 1474-1481

Nishiguchi, T.; Kitabata, H. & Tanaka, A. (2010). Very late stent thrombosis after drug-eluting stent in segment with neointimal tissue coverage. *JACC Cardiovasc Imaging*, Vol. 3, No.4, (April), pp. 445-446

Prati, F.; Regar, E. & Mintz, GS. (2010). Expert review document on methodology, terminology, and clinical applications of optical coherence tomography: physical principles, methodology of image acquisition, and clinical application for assessment of coronary arteries and atherosclerosis. *Eur Heart J*, Vol. 31, No. 4, (February), pp. 401-415

Raffel, OC.; Akasaka, T. & Jang, IK. (2008). Cardiac optical coherence tomography. *Heart,* Vol.94, No.9, (September), pp. 1200-1210

Sawada, T.; Shite, J. & Garcia-Garcia, HM. (2008). Feasibility of combined use of intravascular ultrasound radiofrequency data analysis and optical coherence tomography for detecting thin-cap fibroatheroma. *Eur Heart J*, Vol. 29, No. 9, (May), pp. 1136-1146

Stary, HC. (2000). Natural history and histological classification of atherosclerotic lesions: an update. *Arterioscler Thromb Vasc Biol*, Vol. 20, No. 5, (May), pp. 1177-1178

Takano, M.; Yamamoto, M. & Inami, S. (2009). Appearance of lipid-laden intima and neovascularization after implantation of bare-metal stents extended late-phase observation by intracoronary optical coherence tomography. *J Am Coll Cardiol*, Vol. 55, No. 1, (December), pp. 26-32

Takarada, S.; Imanishi, T. & Kubo, T. (2009). Effect of statin therapy on coronary fibrous-cap thickness in patients with acute coronary syndrome: Assessment by optical coherence tomography study. *Atherosclerosis,* Vol. 202, No.2, (February), pp. 491-497

Takarada, S.; Imanishi, T. & Liu, Y. (2010). Advantage of next-generation frequency-domain optical coherence tomography compared with conventional time-domain system in the assessment of coronary lesion. *Catheter Cardiovasc Interv,* Vol. 75, No.2, (February 1), pp. 202-206

Takarada, S.; Imanishi, T. & Ishibashi, K. (2010). The effect of lipid and inflammatory profiles on the morphological changes of lipid-rich plaques in patients with non-ST-segment elevated acute coronary syndrome: follow-up study by optical coherence tomography and intravascular ultrasound. *JACC Cardiovasc Interv,* Vol. 3, No.7, (July), pp. 766-772

Tanaka, A.; Imanishi, T. & Kitabata, H. (2008). Distribution and frequency of thin-capped fibroatheromas and ruptured plaques in the entire culprit coronary artery in patients with acute coronary syndrome as determined by optical coherence tomography. *Am J Cardiol,* Vol. 102, No.8, (October 15), pp. 975-979

Tanaka, A.; Imanishi, T. & Kitabata, H. (2008). Morphology of exertion-triggered plaque rupture in patients with acute coronary syndrome: an optical coherence tomography study. *Circulation,* Vol. 118, No.23, (December 2), pp. 2368-2373

Tanaka, A.; Imanishi, T. & Kitabata, H. (2009). Lipid-rich plaque and myocardial perfusion after successful stenting in patients with non-ST-segment elevation acute coronary syndrome: an optical coherence tomography study. *Eur Heart J,* Vol. 30, No.11, (June), pp. 1348-1355

Tanimoto, T.; Imanishi, T. & Tanaka, A. (2009). Various types of plaque disruption in a culprit coronary artery visualized by optical coherence tomography in a patient with unstable angina. *Circ J,* Vol. 73, No.1, (January), pp. 187-189

Tearney, GJ.; Yabushita, H. & Houser, SL. (2003). Quantification of macrophage content in atherosclerotic plaques by optical coherence tomography. *Circulation,* Vol. 107, No.1, (January), pp. 113-119

Tearney, GJ.; Waxman, S. & Shishkov, M. (2008). Three-dimensional coronary artery microscopy by intracoronary optical frequency domain imaging. *JACC Cardiovasc Imaging,* Vol. 1, No.6, (November), pp. 752-761

Virmani, R.; Kolodgie, FD. & Burke, AP. (2000). Lessons from sudden coronary death: a comprehensive morphological classification scheme for atherosclerotic lesions. *Arterioscler Thromb Vasc Biol*, Vol. 20, No. 5, (May), pp. 1262-1275

Virmani, R.; Burke, AP. & Kolodgie, FD. (2003). Pathology of the thin-cap fibroatheroma: a type of vulnerable plaque. *J Interv Cardiol*, Vol. 16, No. 3, (June), pp. 267-272

Yabushita, H.; Bouma, BE. & Houser, SL. (2002). Characterization of human atherosclerosis by optical coherence tomography. *Circulation,* Vol. 106, No.13, (September), pp. 1640-1645

Yamaguchi, T.; Terashima, M. & Akasaka, T. (2008). Safety and feasibility of an intravascular optical coherence tomography image wire system in the clinical setting. *Am J Cardiol,* Vol. 101, No.5, (March), pp. 562-567

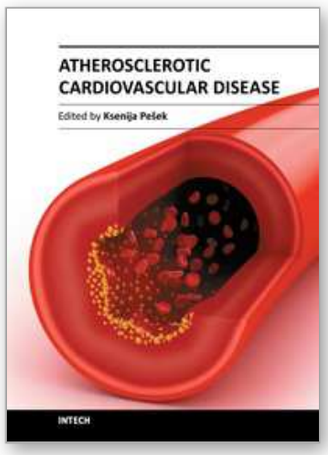


**Atherosclerotic Cardiovascular Disease**
Edited by Dr. Ksenija Pesek

ISBN 978-953-307-695-9
Hard cover, 124 pages
**Publisher** InTech
**Published online** 03, October, 2011
**Published in print edition** October, 2011

Cardiovascular diseases (CVD) are still one of the leading causes of death in the world. The book Atherosclerotic Cardiovascular Disease is a contribution to the application of new knowledge in the area of cardiovascular diseases. The book comprises six chapters divided in three subsections, starting with the General Considerations of Cardiovascular Disease, through Diagnostic Techniques, and Specific Therapy.

**How to reference**
In order to correctly reference this scholarly work, feel free to copy and paste the following:

Takashi Kubo and Takashi Akasaka (2011). Identification of Vulnerable Plaques with Optical Coherence Tomography, Atherosclerotic Cardiovascular Disease, Dr. Ksenija Pesek (Ed.), ISBN: 978-953-307-695-9, InTech, Available from: http://www.intechopen.com/books/atherosclerotic-cardiovascular-disease/identification-of-vulnerable-plaques-with-optical-coherence-tomography

INTECH
open science | open minds

**InTech Europe**
University Campus STeP Ri
Slavka Krautzeka 83/A
51000 Rijeka, Croatia
Phone: +385 (51) 770 447
Fax: +385 (51) 686 166
www.intechopen.com

**InTech China**
Unit 405, Office Block, Hotel Equatorial Shanghai
No.65, Yan An Road (West), Shanghai, 200040, China
中国上海市延安西路65号上海国际贵都大饭店办公楼405单元
Phone: +86-21-62489820
Fax: +86-21-62489821

IntechOpen